Proceedings of the
Annual Stability Conference
Structural Stability Research Council
Louisville, Kentucky, April 1-4, 2025

A low-cost system for enhanced seismic stability and mitigation of residual deformations in steel eccentrically braced frames

Pedram Mortazavi[1], Constantin Christopoulos[2], Oh-Sung Kwon[3]

Abstract
The response of stable yielding systems with enhanced ductility such as steel buckling-restrained braced frames (BRBFs) and eccentrically braced frames (EBFs) often exhibit a seismic response where their peak response is concentrated locally and results in large residual deformations. Gravity induced second-order P-Delta effects influence these response parameters and, in extreme cases, can compromise the global seismic stability of such systems. Furthermore, excessive residual deformations increase the required resources for post-earthquake repairs and elongate the recovery time for damaged structures. For EBFs, which rely on localized inelastic deformations in the yielding link, peak and residual link rotations are much larger than inter-story drift ratios. Recent experimental and numerical studies have shown that even with moderate residual inter-story drift ratios, severe residual link rotations could be expected, which could render the structure difficult to repair even for EBFs with replaceable yielding links. This paper presents the development of a low-cost dual system in EBFs, which is intended to enhance their seismic stability and mitigate their peak and residual deformations. After presenting the design concept, the proposed system is adopted for a prototype EBF designed with cast steel replaceable modular yielding links. The performance of the proposed system is evaluated through nonlinear time-history analyses under a suite of earthquake records. The results demonstrate that the proposed system is effective in increasing the seismic stability of EBFs, reducing both peak and residual deformations. Reduced link residual rotations will result in shorter repair and recovery time after major earthquakes and a more resilient and sustainable design for EBFs.

1. Background

The strength and stiffness of structural steel as a material facilitates the design of slender structural components. This leads to designing structural systems, which are generally flexible in nature compared to other structural systems. In addition, the inherent ductility of steel, along with careful detailing facilitates the design of ductile energy dissipative yielding fuses with enhanced deformation capacity. The flexible nature of steel seismic force resisting systems (SFRSs), combined with their enhanced peak deformation capacity, makes them more prone to gravity-induced second-order P-Delta effects. P-Delta effects can further increase both peak and residual

[1] Assistant Professor, University of Minnesota, <pmortaza@umn.edu>
[2] Professor, University of Toronto, <c.christopoulos@utoronto.ca>
[3] Professor, University of Toronto, <os.kwon@utoronto.ca>

deformation demands and, in some extreme cases, can compromise the global seismic stability of the frame structure. As such, stable yielding systems with enhanced ductility are susceptible to experiencing large residual deformations. This has previously been shown for single degree of freedom and multi degree of freedom systems (MacRae and Kawashima 1998; Christopoulos et al. 2003; Pampanin et al. 2003, Christopoulos et al. 2004). Detailed numerical studies on ductile steel SFRSs such as special moment resisting frames (SMRFs) and buckling-restrained braced frames (BRBFs) have also confirmed these observations (Sabelli et al. 2003; Fahnestock et al. 2007a; Tremblay et al. 2008; Erochko et al. 2011), which are also supported by experimental studies (Fahnestock et al. 2007b; Mojiri et al. 2021; Mortazavi et al. 2022). Recent investigations into the behavior of eccentrically braced frames (EBFs) have provided critical insights through both numerical and experimental studies. Mortazavi et al. (2024a) conducted a numerical analysis on EBFs ranging from 2 to 12 stories, comparing conventional EBFs with systems incorporating cast steel replaceable yielding links (Mortazavi et al. 2023a; 2023b). Their performance was assessed under a suite of forty earthquake ground motions, showing that EBFs tend to develop significant residual drifts, with even larger residual link rotations. Notably, at the DBE-level hazard, 75% of the cases exhibited link residual rotations exceeding 0.005 radians. Additionally, 50% to 70% of the analyzed structures experienced residual link rotations surpassing 0.01 to 0.02 radians, posing substantial challenges for link replacement. The study also highlighted that in EBFs, residual link rotations can be critical even when overall building drifts remain moderate (i.e., below 0.5%), due to the localization of inelastic deformations within the yielding links. These findings were further confirmed in an experimental study where two low-rise prototype EBFs, incorporating cast steel replaceable modular yielding links, were evaluated through pseudo-dynamic hybrid simulations under earthquake excitations (Mortazavi et al. 2023c). Both building structures exhibited excessive residual deformations, with localization of residual rotations within the yielding link.

Excessive residual deformations can compromise a building's functionality and, in extreme cases, result in its total economic loss. McCormick et al. (2008) provide guidelines on acceptable residual deformations in structural systems, suggesting that residual rotations or drifts exceeding 0.005 radians (0.5%) become perceptible to occupants. Furthermore, when these values surpass 0.01 radians, they can cause discomfort and significantly impede the building’s usability. In the case of steel EBFs with replaceable yielding links, excessive residual link rotations can hinder the replacement of the yielding links and times make it impossible, and therefore, increase the building recovery and repair time after an earthquake.

Given the significant impact of residual deformations on a building's post-earthquake functionality, significant research has been conducted on the development of self-centering structural systems, as outlined in Zhong and Christopoulos (2021). Full self-centering behavior, which is shown in Figure 1 (a), can be achieved through several methods including (1) the use of shape memory alloy materials (DesRoches et al. 2004; Ocel et al. 2004; Zhang and Zhu 2007; Youssef et al. 2008; Attanasi et al. 2009; Ozbulut and Hurlebaus 2010; Bhuiyan and Alam 2013; Qian et al. 2016; Alipour et al. 2017; Zareie et al. 2020), (2) Mechanical systems or post-tensioned devices (Christopoulos et al. 2002; Christopoulos et al. 2008; Bishay-Girges and Carr 2014; Erochko et al. 2015; Xu et al. 2018; Hashemi et al. 2018; Bagheri et al. 2020), (3) Use of geometry by incorporating rocking mechanisms (Dowden and Bruneau 2011; Deierlein et al. 2011; Calugaru 2013; Eatherton et al. 2014; Wiebe and Christopoulos 2015; Bahmani et al. 2017; Binder and

Christopoulos 2018; Kashani et al. 2018), and, (4) A combination thereof (Ma et al. 2011; Miller et al. 2012; Hashemi et al. 2017; Hashemi et al. 2018). While these methods have proved effective in eliminating residual deformations and enhancing the resilience of structures, they are more costly and more technically complex when compared to conventional structural systems, making their implementation more challenging. An alternative approach is the use of dual systems, which provide additional global post-yield stiffness from the elastic response of the back-up system. The elastic response of the backup system provides a restoring force which can reduce or eliminate second-order P-Delta effects and enhances the global seismic stability of the steel frame. Dual systems, which are conceptually shown in Figure 1 (b), have been shown to be quite effective in mitigating both peak and residual deformations (Uang and Kiggins 2008; Gupta and Krawinkler 1999; Alavi and Krawinkler 2004; Lignos and Elkady 2015).

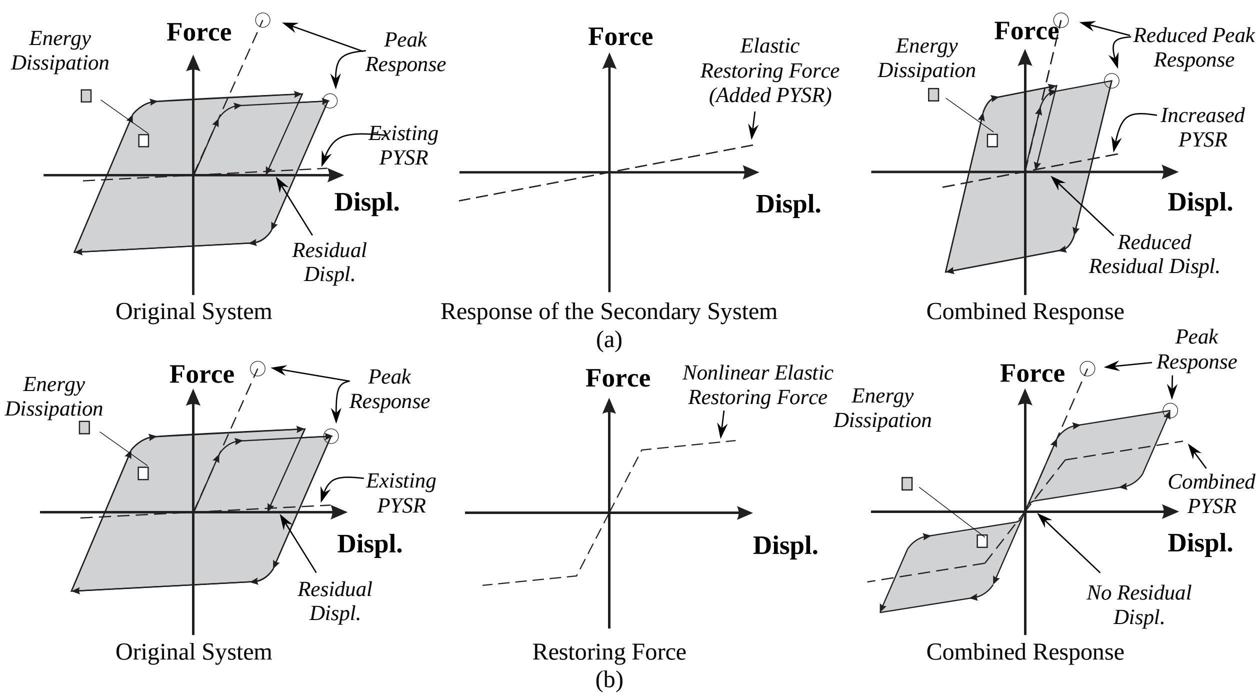

Figure 1: (a) Response of a Dual System, and (b) Response of a Self-Centering System

This study presents a low-cost dual system for use in steel EBFs for enhancing the global seismic stability of EBFs and for mitigating their peak and residual deformations. A proof of concept was recently validated through pseudo-dynamic hybrid simulations (Mortazavi et al., 2024b). This paper is focused on a comprehensive numerical study on a reference structure, which adopts the proposed system. The proposed dual system, its mechanics, and design considerations are first presented. The design of a reference EBF structure, which is designed with the recently developed cast steel replaceable modular yielding links is presented. The suite of ground motions that are used in the study are presented. The proposed dual system is adopted for the reference structure. Numerical models of the reference structure, with and without the proposed dual system, are developed. The reference structure is then studied through nonlinear time history analyses. The results from the analyses are compared between the original prototype structure and the upgraded structure.

2. Proposed Dual System

2.1 Overview

A 3-dimensional rendering of the proposed dual system is shown in Figure 2 (a). The design involves having two hollow structural steel (HSS) sections installed in parallel with the yielding link, as shown in Figure 2 (a). HSS members are used to avoid lateral torsional buckling. The cast steel link was also designed to feature tapered hollow box regions to facilitate distributed plasticity and to avoid lateral torsional buckling, and the need to laterally restrain the yielding link from lateral torsional buckling. One design aspect that had to be addressed was to make sure that the HSS beams do not impose any axial restraint on the yielding link. As such, the end connections were especially detailed with slotted holes, as shown in Figure 2 (b) and (c), to transfer the flexural moments but allow axial movement. The middle-slotted hole is used to transfer the shear demand, while the exterior ones are used to transfer the flexural demands. The sleeve connection is welded to an endplate, which is connected to *adapter connections* using high-strength bolts. The adapter connections are shop welded to the floor beam. As the system deforms, the HSS beams undergo lower localized rotations given that they are longer than the yielding links. Therefore, they maintain their elastic stiffness for a larger portion of the response. The elastic stiffness of the HSS beams will then generate a post-yield stiffness for the global response of the EBF, which can enhance the seismic stability of the system and reduce its peak and residual deformations. The proposed dual system has three main advantages: (1) The system relies on auxiliary HSS elements as the backup system, which can easily be replaced if they experience yielding in extreme events, (2) It decouples the added stiffness at each floor (i.e., different HSS size beams can be added at each floor), and (3) The proposed design does not impose a significant change to the architectural layout of the building and can easily be adopted for both new and existing EBFs.

2.2 Mechanics

Figure 2 (d) shows an undeformed state of the system, where e_y represents the yielding length of the link, and e_{HSS} denotes the length of the HSS member. The corresponding deformed shape is depicted in Figure 2 (e), demonstrating that the vertical deformations of both the yielding link and the HSS beams are equal ($\Delta_{Link} = \Delta_{HSS}$). Therefore, they perform as two springs in parallel.

Before yielding, the lateral stiffness of the EBF is influenced by all structural components, including the yielding link, columns, beams, and braces. However, once the link undergoes yielding, the global response is primarily driven by the yielding link, while the beam-column-brace assemblies rotate as rigid bodies. In this system, the HSS beams contribute to the post-yield behavior, meaning their dimensions can be selected to achieve the desired post-yield stiffness ratio (PYSR), K_{Req}. Since the HSS beams are substantially longer than the yielding links, their response is dominated by flexural deformations, with shear deformations being negligible. Given their boundary conditions, the stiffness of the HSS member can be determined as follows:

$$K_{Req.}/2 = K_{HSS} = \left(\frac{12E_{HSS}I_{HSS}}{e_{HSS}{}^3}\right) \tag{1}$$

where E_{HSS} is the modulus of elasticity of the steel material of the HSS beams, I_{HSS} is the moment of inertia of the HSS beam about its axis of bending, and e_{HSS} is the length of the HSS beams.

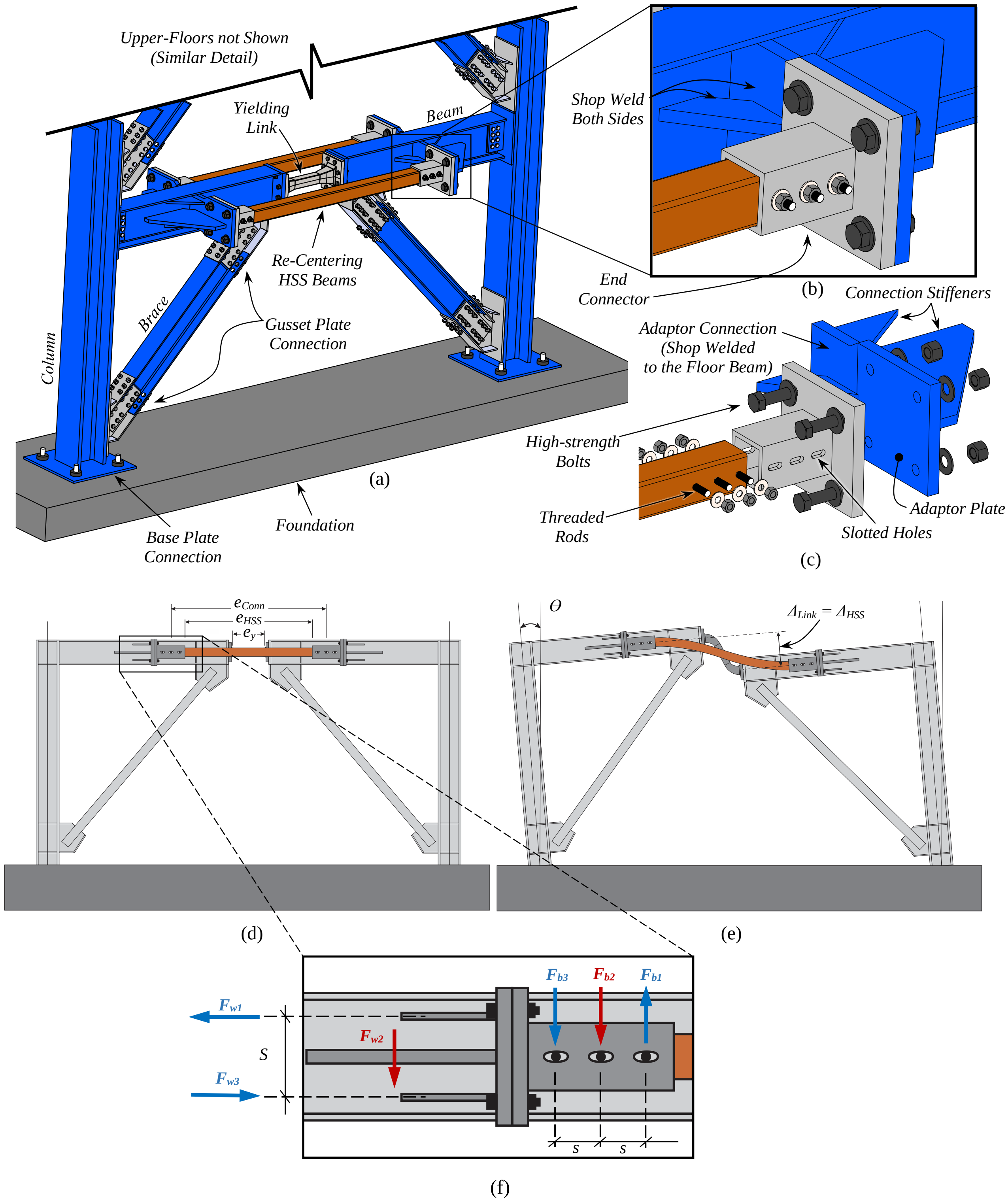

Figure 2: Proposed Re-Centering System: (a) 3D Rendering, (b) Connection Detail, (c) Connection Parts, (d) Undeformed Shape, (e) Deformed Shape, and (f) Connection Design Forces

The required stiffness (K_{req}) can be selected to target a desirable PYSR. For instance, K_{Req} can be selected to counter the negative stiffness caused by P-Delta effects. While specifying the target K_{Req}, the length of the HSS member (L_{HSS}) can be selected. Afterwards, the required moment of inertia of the HSS member (I_{HSS}) is determined from Equation (1). It must be noted that K_{HSS} in Equation (1) is taken as half of K_{Req}, given that the system incorporates two HSS members. Several factors can be considered when specifying the HSS beam's length, depth, and material yield strength, which will be discussed in Section 2.3.

The proposed connection detail for attaching the HSS member to the floor beam is illustrated in Figure 2 (f), along with the design forces acting on the bolts within the slotted holes. In practice, the shear force from the HSS member is evenly distributed among the three bolts. However, the bending moment is primarily transferred through the two outer bolts. For design purposes, as a conservative approach the central bolt is designed to carry the entire shear force associated with the probable flexural capacity of the HSS beam (i.e., $F_{b2} = V_{pr\text{-}HSS} = M_{pr\text{-}HSS}/e_{Conn}$, where e_{Conn} is the distance between the two end connections as shown in Figure 2 (d)). The two side bolts are designed to resist the probable moment capacity of the HSS beam (M_{pr-HSS}) through a couple action, in addition to carrying one-third of the total shear force (i.e., $F_{b1} = F_{b3} = M_{pr\text{-}HSS} /2s + V_{pr\text{-}HSS}/3$, where s is the horizontal distance between the bolts). The forces acting on the welds connecting the adapter plate to the floor beam are also shown in Figure 2 (f). The welds on the top and bottom stiffeners are designed to resist the force associated with the probable bending moment capacity of the HSS beam (i.e., $F_{w1} = M_{pr\text{-}HSS} /S$, where S is the vertical distance between the two stiffeners). The remaining welds including the welds on the middle stiffener and the weld on the adapter plate (see Figure 2) are relied upon to transfer the shear force from the HSS beam. Alternative connection details may also be used, provided they effectively transfer moment and shear while preventing axial restraint.

2.3 Design Considerations

The HSS beams should be sufficiently long to ensure a flexural-dominant behavior. However, when targeting a specific post-yield stiffness, excessively increasing the length of the HSS would require a heavier section to maintain the same vertical stiffness. Additionally, significantly longer HSS beams could generate higher bending moments at their ends, increasing the demands on the end connections. Therefore, selecting an appropriate HSS length requires engineering judgment. Based on initial design iterations and subsequent analyses, an optimal $e_{\_HSS}$ typically falls between $3{\times}e_y$ and $6{\times}e_y$. This range helps ensure that the end moments of the HSS beams are transferred to the adjacent beams outside the link in regions with minimal bending moment (i.e., near the moment diagram's inflection points when the link is yielding). Furthermore, this range facilitates efficient and practical detailing of the HSS end connections for most EBF configurations.

Another design aspect is choosing the depth of the HSS beams. If two HSS members with different depths have the same length and moment of inertia, they will undergo identical rotations and curvatures under a given EBF global deformation. However, the deeper HSS section will experience greater strain at its extreme fibers. As a result, a deeper HSS beam is more likely to yield at a lower link rotation, thereby eliminating the intended post-yield stiffness contribution at an earlier stage of the response. To ensure the HSS remains elastic up to the target link rotation (i.e., 0.09 radians of total rotation), its depth must be carefully selected.

The yield threshold of the HSS beams can also be adjusted by selecting higher-strength HSS sections. While HSS members with yield strengths of 300–350 MPa are more commonly used, higher-strength options with yield strengths of 700 MPa, 900 MPa, 1100 MPa, and even 1300 MPa may be available commercially (Ma et al. 2017). These higher-strength materials can be utilized to control the yield initiation of the HSS beams relative to the yielding link's rotation. In North America, HSS grades with yield strengths of 485 MPa, 550 MPa, 620 MPa, 690 MPa, and 760 MPa are more readily accessible (AISC 2018) and can be incorporated into design applications as needed.

3. Prototype Building Structure

3.1 Original Building Design

The prototype structure is a four-story office building located in downtown Los Angeles on site class C, designed and detailed by Mortazavi et al. (2023c). The building is shown in Figure 3. The seismic force-resisting system (SFRS) in the north-south direction is formed by special moment-resisting frames (SMRFs). In the east-west direction, the SFRS is formed by eight eccentrically braced frames (EBFs). The EBFs were designed with cast steel modular yielding links. The structural design followed the ASCE 7-16 standard (2016), with modifications for the implementation of cast steel links in the EBFs (Mortazavi 2023). Notably, the maximum allowable link rotation was increased to 0.12 radians due to the enhanced rotational capacity of cast steel links. All steel components were designed and detailed per AISC 360-16 (2016) and AISC 341-16 (2016). The cast steel yielding links were sized to have a nominal plastic shear capacity of 445 kN in floors one and two, 343 kN on the third floor, and 200 kN on the fourth floor. The EBF columns below the splice were designed as W310×79 sections, while those above the splice were W310×45. The braces were specified as W200×71 sections for the first and second floors, with W200×52 and W200×46 sections for the third and fourth floors, respectively. The beams were selected as W410×67, W410×60, W360×51, and W250×39 for stories one through four, respectively. The building's seismic weight was determined to be 4321 kN, 4308 kN, 4292 kN, and 3633 kN for floors one through four, resulting in a total seismic weight of 16,550 kN.

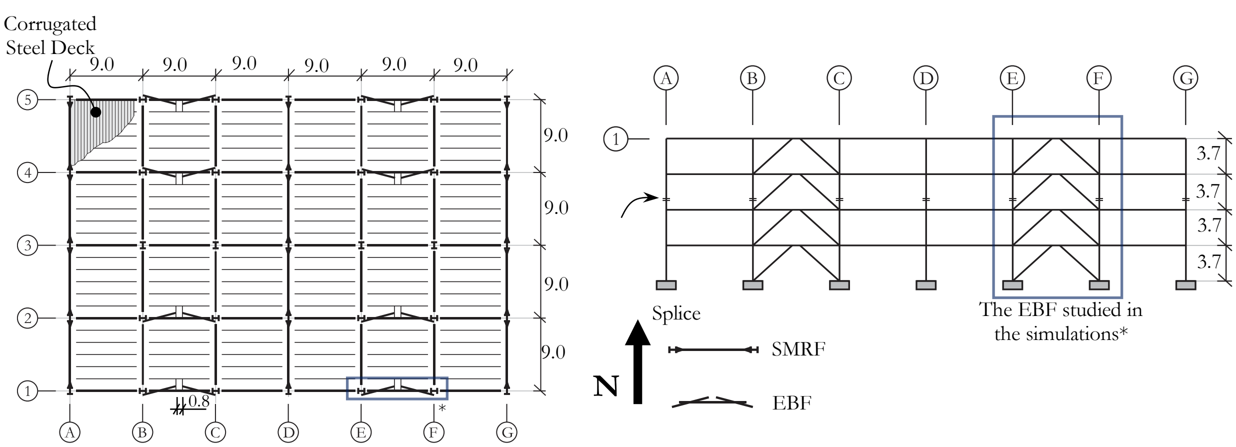

Figure 3: Illustration of the Prototype Four-Story Office Building with Steel EBFs (all dimensions in meters)

3.2 Adoption of the Dual System for the Reference Building

The elastic stiffness of the cast steel yielding links that were used in the reference EBF were 85 kN/mm for the first and second floor, 67.5 kN/mm for the third floor, and 38 kN/mm for the fourth floor. After a thorough parametric study, the optimum post yield stiffness ratio was determined to be between 7% to 7.5% (Mortazavi et al. 2024b). The inherent post-yield stiffness of cast steel replaceable links is approximately 3.5% determined from experimental results. Consequently, the two HSS members at each floor must be selected to contribute an additional 3.5% to 4% post-yield stiffness to the yielding link. The HSS beam length was set at four times the yielding link length (i.e., $e_{HSS} = 4 \times e_y = 2845$ mm). Using a required stiffness ($K_{Req.}$) equal to 4% of the yielding link's elastic stiffness, the moment of inertia of the HSS beams (I_{HSS}) is determined, and HSS sections are selected. The selected HSS sections are summarized in Table 1.

Table 1: Design of the Dual System

Yielding Links	$e_{HSS} = 4 \times e_y$ (used in the design)				
	HSS Section	**I_{HSS} (mm^4)** *	**Added PYSR (%)** **	**γ_{Link} (M_y)** ⸸	**γ_{Link} (M_p)** †
EBF100	HSS178×127×6.4	15.8×10^6	3.9	0.096	0.116
EBF77	HSS178×127×4.8	12.4×10^6	3.8	0.096	0.116
EBF45	HSS152×76×6.4	7.47×10^6	4.1	0.112	0.143

**Moment of inertia for one HSS beam*

***Added post-yield stiffness at each floor from both HSS beams*

⸸ Link rotation associated with HSS beam reaching M_y reported for $F_{y\text{-}HSS} = 900$ MPa

† Link rotation associated with HSS beam reaching M_p reported for $F_{y\text{-}HSS} = 900$ MPa

The HSS end bending moment (M_{HSS}) can be found using Equation (2), given an assumed flexural dominant response in double curvature for the HSS beams. In Equation (2), Δ is the vertical deformation of the HSS beams, which is equal to the vertical deformation of the yielding link. Therefore, Δ can be expressed as shown in Equation (3). In addition, M_{HSS} can be replaced with the plastic moment capacity of the HSS beams ($M_{p\text{-}HSS}$), as shown in Equation (4).

$$M_{HSS} = \left(\frac{6.E_{HSS}.I_{HSS}}{{e_{HSS}}^2}\right).\Delta \tag{2}$$

$$\Delta = \gamma_{Link}.e_y \tag{3}$$

$$M_{p-HSS} = Z_{HSS}.F_{y-HSS} \tag{4}$$

In the above equations, E_{HSS} is the modulus of elasticity of the HSS steel material, I_{HSS} is the moment of inertia of the HSS beam, e_{HSS} is the length of the HSS beam, γ_{Link} is the rotation of the yielding link, e_y is the length of the yielding link, $F_{y\text{-}HSS}$ is the yield strength of the HSS material, and Z_{HSS} is the plastic section modulus of the HSS beams.

Assuming an idealized elastoplastic response for the HSS beams and substituting Equations (3) and (4) into Equation (2), a relationship between the material yield strength of the HSS beams and the link rotation at which the HSS beams has reached its plastic moment capacity can be obtained, which is given in Equation (5).

$$\gamma_{Link} = \left(\frac{Z_{HSS}.F_{y-HSS}.{e_{HSS}}^2}{6.E_{HSS}.I_{HSS}.e_y}\right) \tag{5}$$

The link rotation that is obtained from Equation (5) is the rotation beyond which the HSS beams reach their plastic moment capacity. Therefore, after this link rotation the HSS beams will not provide the system with any significant post-yield stiffness.

The dual system adopted for the reference structure was designed with HSS members with different grades of steel to evaluate the effect of yield stress on the response. The yield stress values that were used in the design included 700 MPa, 900 MPa, 1100 MPa, and 1300 MPa. The link rotation at which the secondary HSS beams yield for each steel grade are shown in Figure 4. The yield rotation is also shown for $F_{y\text{-}HSS}$ = 350 MPa as a common yield strength for most steel grades, which shows the effectiveness of using higher steel grades. Alternatively, the HSS beams can be designed to be longer (i.e., 5×e_y or 6×e_y) to increase the rotation range in which the HSS beam stays elastic.

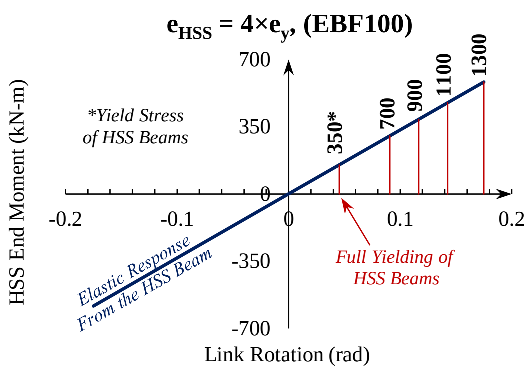

Figure 4: Effect of Increasing $F_{y\text{-}HSS}$ on the Elastic Response Range

4. Seismicity and Ground Motions

The ground motions used in the study are shown in Figure 5, which were originally selected and scaled to be representative of the seismicity of downtown Los Angeles and match the design target spectrum of the site over an extended period range, covering the period range of interest for the reference structures as well (i.e., 0.2$T1$ – 2.0$T1$). The suite of ground motions includes 40 records from the Pacific Earthquake Engineering Research Centre (PEER) ground motion database (PEER 2020). The complete list of ground motions and scale factors used are provided by Mortazavi et al. (2024a).

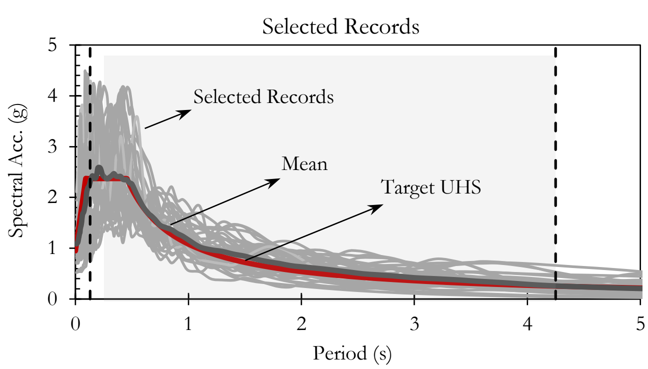

Figure 5: PSA of the Suite of Ground Motions used in the Study

5. Seismic Performance Assessment

5.1 Modelling Approach

The modeling approach for cast steel yielding links follows the methodology proposed by Mortazavi et al. (2023c). As illustrated in Figure 6, the links are represented in OpenSees using a series of *forceBeamColumn* elements with fiber sections to capture both the flexural and axial behavior, including their interaction. The shear response of each section is separately modeled and incorporated using a section aggregator command. The elastic segment of the link is represented by a single *forceBeamColumn* element, while the yielding region is discretized into eleven elements to account for the tapering in this area.

The steel material is modeled using the Steel02 (GMP) material in OpenSees, with parameters b, *Ro*, *cR1*, *cR2*, *a1*, *a2*, *a3*, and *a4* set to 0.003, 20, 0.92, 0.15, 0.025, 1, 0.025, and 1, respectively. The modulus of elasticity and yield strength of the steel are taken as 200,000 MPa and 330 MPa, based on coupon test results. Additionally, the link end plates are modeled as rigid elements. Further details on the modeling approach can be found in Mortazavi et al. (2023c).

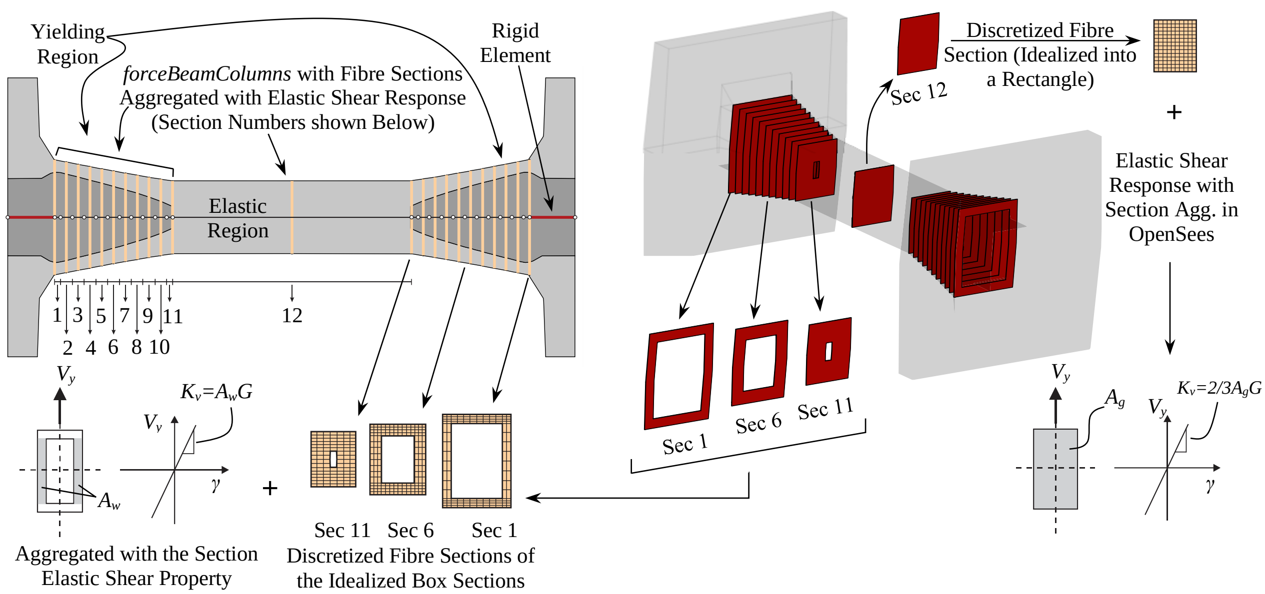

Figure 6: Numerical Modelling Approach for Cast Steel Replaceable Modular Yielding Links

The global modelling approach for the reference EBF is shown in Figure 7, which was modeled in OpenSees. Since the structure is symmetrical in plan, torsional effects were ignored, and a two-dimensional model was developed. The seismic mass for each floor was distributed equally as *M*/2 to each node.

To account for global P-Delta effects, an elastic leaning column was included in the numerical model, with a weight corresponding to one-eighth of the total building weight. The beams, columns, braces, and HSS beams were modeled using *beamWithHinges* elements with fiber sections. The steel material for elements outside the links was modeled using the *Steel02* material with a 2% post-yield stiffness and a yield stress of 345 MPa. The parameters *Ro*, *cR1*, and *cR2* were taken as 18, 0.925, and 0.15, respectively (Mojiri et al., 2021), while additional hardening parameters were assigned default values. The yield strength for the HSS beams was taken as the design values discussed earlier.

All connections were modeled as rigid, except for the base column connections. Proper rigid end offsets were included to account for the additional stiffness at the intersection of beams and columns and the presence of gusset plates. The HSS beam-to-floor beam connections were modeled to restrain shear and bending moment actions while allowing free axial movement.

The periods of the first two modes of vibration for the reference EBF were found to be 0.53 s and 0.21 s without the HSS beams. After incorporating the HSS beams, the periods changed slightly to 0.526 s and 0.207 s. This negligible change in structural periods confirms that the added stiffness of the HSS beams does not significantly alter the elastic stiffness of the structure, ensuring that the design base shear remains nearly unchanged. An inherent viscous damping of 3% was assumed in the first two modes in the numerical model.

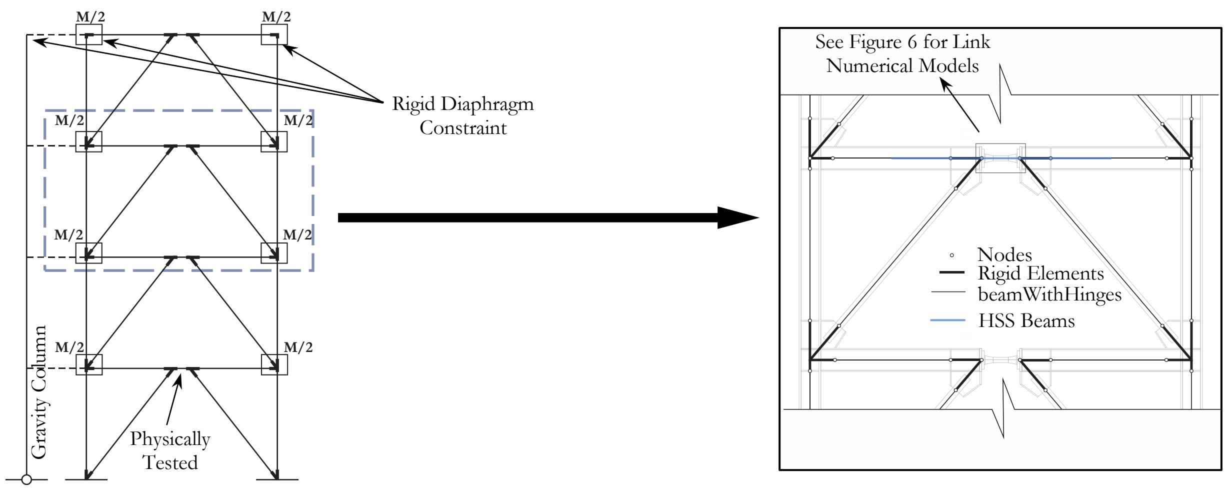

Figure 7: Illustration of the Global Numerical Model

5.1 Results

The response of the reference structure, with and without the dual system, is evaluated under the suite of selected and scaled ground motions at both design basis earthquake (DBE) level and the maximum credible earthquake (MCE) level. For the design featuring the proposed dual system, the response is evaluated with different yield strengths for the HSS beams including 700 MPa, 900 MPa, 1100 MPa, and 1300 MPa. The mean values of maximum transient and residual drifts, and maximum and residual link rotations along the building height are shown in Figure 8 for each design. Both transient drifts and link rotations are reduced as a result of using the proposed dual system. As can be observed, the residual drifts are controlled effectively, even at the MCE level, with the mean value being less than the threshold of being perceivable by the building occupants (i.e., less than 0.5%). Residual link rotations are also controlled well. As expected, the largest reduction was obtained for the HSS with the highest grade of steel. Previous experimental studies on EBFs with cast steel replaceable yielding links have shown that even after three back-to-back MCE level records, the yielding links can still survive the loading protocol for qualification of EBF links. Therefore, given that the global residual drift levels are well below levels that would be perceivable by occupants, replacing the link may not be necessary and the building may continue to be used after repairs to non-structural elements. Using longer HSS beams (i.e., 7×e_y) can further reduce the residual link rotations, to remove the need for any re-centering even after an MCE level earthquake.

The response of the reference structure with and without the dual system under the DBE level suite of records is shown in Figure 9. A similar trend is observed in the response, but with a more effective reduction in residual drifts and residual link rotations, with the latter reduced to a level that replacing the yielding link can be achieved without the need to re-center the structure.

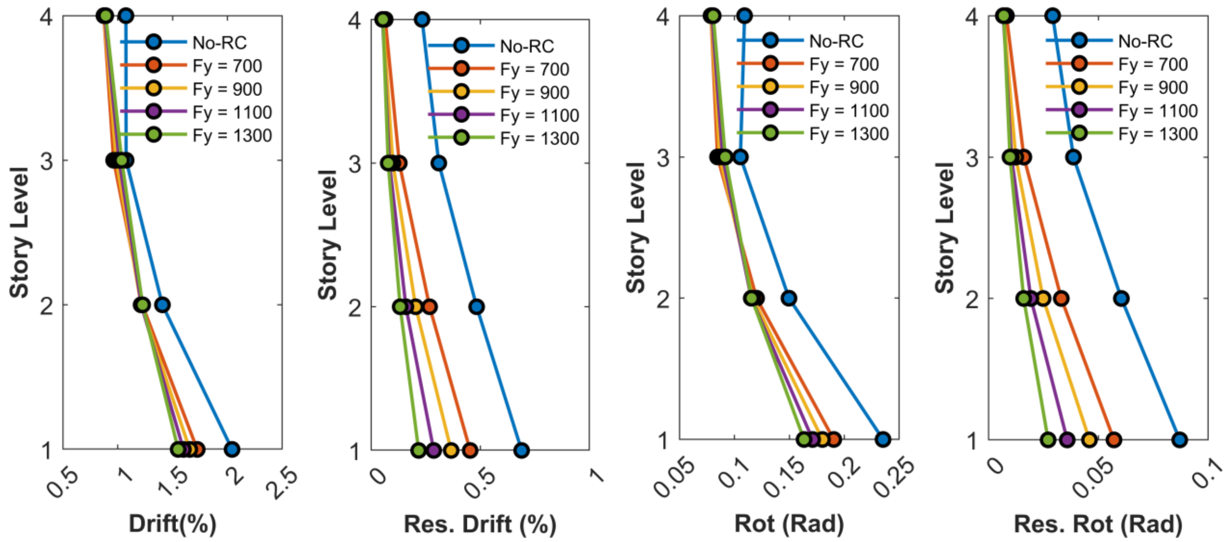

Figure 8: Response of the Reference Structure with and without the Re-Centering Mechanism under the MCE-Level Earthquakes: (a) Drift, (b) Residual Drift, (c) Link Rotation, and (d) Residual Link Rotation

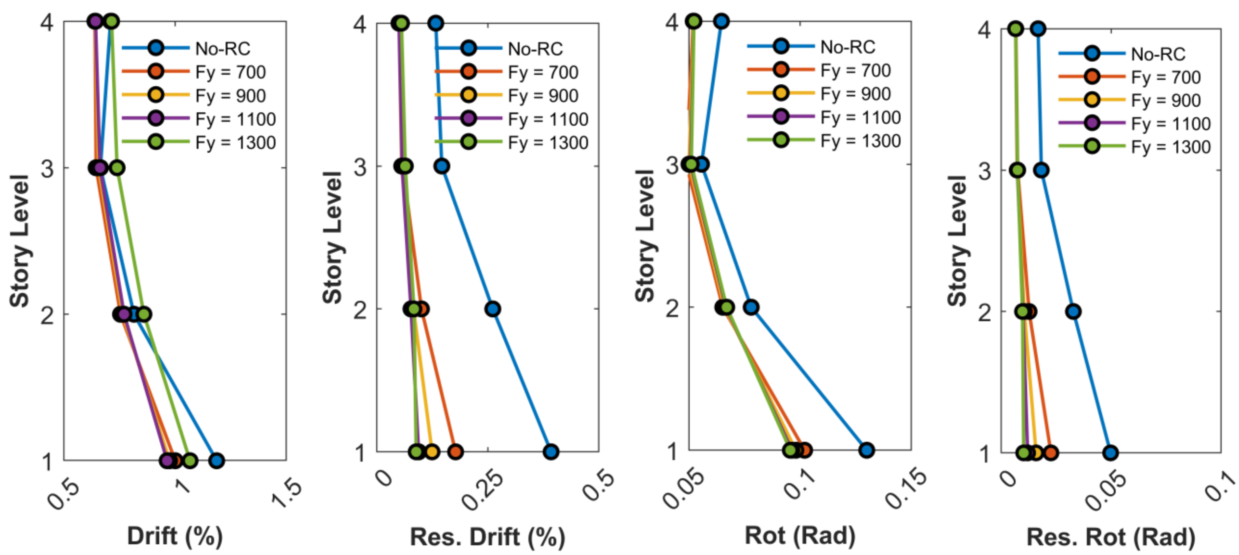

Figure 9: Response of the Reference Structure with and without the Re-Centering Mechanism under the DBE-Level Earthquakes: (a) Drift, (b) Residual Drift, (c) Link Rotation, and (d) Residual Link Rotation

The acceleration response along the height is shown in Figure 10 at both MCE and DBE level hazards. The results show that using the proposed dual system increases the accelerations along the heigh by almost 20%. Therefore, the acceleration response must carefully be examined when adopting dual systems, especially in buildings housing sensitive equipment where an increase in acceleration levels can be critical.

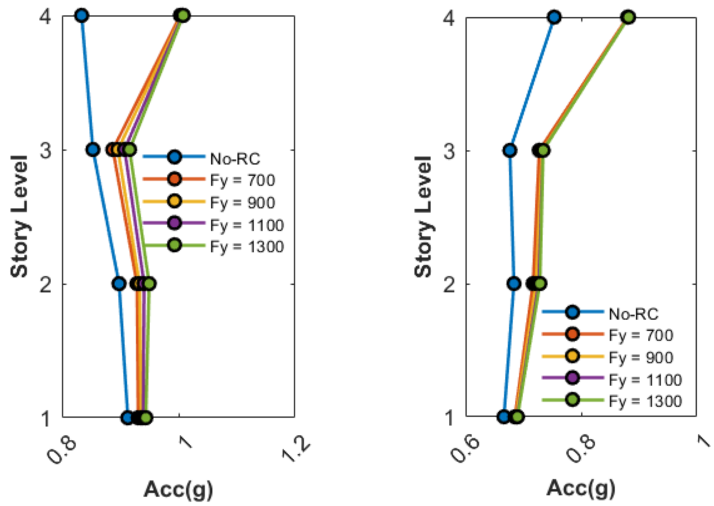

Figure 10: Acceleration Response of the Reference Structure with and without the Re-Centering System at (a) MCE-Level Shaking, and (b) at DBE-Level Shaking

6. Summary and Conclusions

This paper presents a numerical study on a recently proposed dual system for steel EBF structures (Mortazavi et al 2024b), with the aim to mitigate global and local residual deformations. The proof of concept of the proposed system was recently validated through hybrid simulations using only three earthquake records. In the present study the response of a four-story reference EBF building was evaluated under a large set of earthquake records, with and without the proposed dual system, to assess whether the findings from the previous hybrid simulations can be extended to a larger set of earthquakes. The study leads to the following conclusions.

- The proposed system is effective in enhancing the global seismic stability of the system. This is evident given that the proposed system was effective in reducing both peak and residual deformations in the system at MCE and DBE level shakings.

- The dual system reduced the global residual deformations (drifts) to levels that are not perceivable by the occupants (i.e., less than 0.5%). Therefore, if cumulative plastic demand experienced by the yielding links are minimal, the building can continue to be operational after an MCE level earthquake without the need for major structural repairs. The residual link rotations at the MCE level are also reduced. Therefore, replacing the yielding links would be much simpler compared to the original design without the dual system

- At the DBE level shaking, the proposed dual system reduced the residual link rotation values to levels that makes them replaceable after an earthquake.

- The only drawback when using the dual system is an increase in accelerations. In particular, it was shown that the accelerations along the height can increase by up to 20%.

- The results from this numerical study with a large set of earthquake records are consistent with that observed in previous hybrid simulations on the same dual system with only three earthquake records.

Acknowledgments

The authors acknowledge the support of the Natural Sciences and Engineering Research Council of Canada (NSERC) [ALLRP 560261-20] and Ontario Centres of Excellence [OCE VIP II-27058].

References

AISC (American Institute of Steel Construction). 2018. Cold-Formed Welded High Strength Carbon Steel or High-Strength Low-Alloy Steel Hollow Structural Sections (HSS) in Rounds and Shapes. A1112/A1112M-18.

Alavi, B., Krawinkler, H. Effects of near-fault ground motions on frame structures, Report No. 138, Dept. of Civil and Environmental Engineering, Stanford University.

Alipour A, Kadkhodaei M, Safaei M. 2017. Design, analysis, and manufacture of a tension–compression self-centering damper based on energy dissipation of pre-stretched superelastic shape memory alloy wires, Intelligent Material Systems and Structures 28(15): 2129–2139.

American Institute of Steel Construction (AISC), *Load and resistance factor design specification for structural steel buildings, ANSI/AISC 360-16 Including supplement No.1*. Chicago: American Institute of Steel Construction, Inc, 2016.

American Institute of Steel Construction (AISC), *Seismic provisions for structural steel buildings, ANSI/AISC 341-16 Including supplement No.1*. Chicago: American Institute of Steel Construction, Inc, 2016

American Society of Civil Engineers (ASCE), *Minimum design loads for buildings and other structures, ASCE/SEI 7-10, Including supplement No.1*. Reston, VA.: American Society of Civil Engineers, 2016.

Attanasi G, Auricchio F, and Fenves GL, 2009. Feasibility assessment of an innovative isolation bearing system with shape memory alloys, Journal of Earthquake Engineering 13: 18–39.

Bagheri H, Hashemi A, Yousef-Beik SMM, Zarnani P, Quenneville P. 2020. New self-centering tension-only brace using resilient slip-friction joint: Experimental tests and numerical analysis. Journal of Structural Engineering 146(10): 04020219.

Bahmani P, Van de Lindt J, Iqbal A, Rammer D. 2017. Mass timber rocking panel retrofit of a four-story soft-story building with full-scale shake table validation. Buildings 7(2): 48.

Bhuiyan AR, Alam MS. 2013. Seismic performance assessment of highway bridges equipped with superelastic shape memory alloy-based laminated rubber isolation bearing. Engineering Structures 49: 396–407.

Binder J, Christopoulos C. 2018. Seismic performance of hybrid ductile-rocking braced frame system. Earthquake Engineering and Structural Dynamics 47(6): 1394–1415.

Bishay-Girges NW, Carr AJ. 2014. Ring spring dampers. Bulletin of the New Zealand Society for EQ Eng. 47(3): 173–180

Calugaru V. 2013. Earthquake resilient tall reinforced concrete buildings at near-fault sites using base isolation and rocking core walls. Doctoral dissertation, UC Berkeley, Berkeley, CA.

Christopoulos C, Filiatrault A, Uang CM, Folz B. 2002. Posttensioned energy dissipating connections for moment-resisting steel frames. Journal of Structural Engineering 128(9):1111–1120.

Christopoulos C, Tremblay R, Kim HJ, Lacerte M. 2008. Self-centering energy dissipative bracing system for the seismic resistance of structures: Development and validation. Journal of Structural Engineering 134(1): 96–107.

Christopoulos, C., Pampanin, S. 2004. Towards performance-based seismic design of MDOF structures with explicit consideration of residual deformations, *ISET Journal of Earthquake Technology*, Paper No. 440, Vol. 41, No. 1, pp. 53-73.

Christopoulos, C., Pampanin, S., Priestley, N. 2003. Performance-based seismic response of frame structures including residual deformations. Part I: Single degree of freedom systems, Journal of Earthquake Engineering, Vol (7), No. 1, 97-118.

Combescure D. Pegon P. α-Operator splitting time integration technique for pseudodynamic testing error propagation analysis. Soil Dyn Earthquake Eng. 1997; 16(7– 8): 427-443. DOI:10.1016/S0267-7261(97)00017-1

Deierlein G, Krawinkler H, Ma X, Eatherton M, Hajjar J, Takeuchi T, Midorikawa M. 2011. Earthquake resilient steel braced frames with controlled rocking and energy dissipating fuses. Steel Construction 4(3): 171–175.

DesRoches R, McCormick J, Delemont M. 2004. Cyclic properties of superelastic shape memory alloy wires and bars. Journal of Structural Engineering 130(1): 38–46.

Dowden DM, Bruneau M. 2011. NewZ-BREAKSS: Post-tensioned rocking connection detail free of beam growth. Engineering Journal 48(2): 153–158.

Eatherton MR, Ma X, Krawinkler H, Deierlein GG, Hajjar JF. 2014. Quasi-static cyclic behavior of controlled rocking steel frames. Journal of Structural Engineering 140(11): 04014083

Erochko J, Christopoulos C, Tremblay R, Choi H. Residual drift response of SMRFs and BRB frames in steel buildings according to ASCE 7-05. *Journal of Structural Engineering, 2011; 137 (5),* 589-599.

Erochko J, Christopoulos C, Tremblay R. 2015. Design, testing, and detailed component modeling of a high-capacity self-centering energy-dissipative brace. Journal of Structural Engineering 141(8): 04014193.

Fahnestock, L. A., Sause, R., and Ricles, J. M. 2007a. Seismic response and performance of buckling-restrained braced frames. J. Struct. Eng., 133(9), 1195–1204.10.1061/(ASCE)0733-9445(2007)133:9(1195)

Fahnestock, L. A., Ricles, J. M., and Sause, R. 2007b. Experimental evaluation of a large-scale buckling-restrained braced frame. J. Struct. Eng., 133(9), 1205–1214.10.1061/(ASCE)0733-9445(2007)133:9(1205)

Gupta, A. and Krawinkler, H., Seismic demands for the performance evaluation of steel moment resisting frame structures, Report No. 132, The John A. Blume Earthquake Engineering Center, Stanford University, CA, 1999.

Hashemi A, Zarnani P, Darani FM, Valadbeigi A, Clifton GC, Quenneville P. 2018. Damage avoidance self-centering steel moment resisting frames (MRFs) using innovative resilient slip friction joints (RSFJs). Key Eng. Materials 763: 726–734.

Hashemi A, Zarnani P, Masoudnia R, Quenneville P. 2017. Seismic resistant rocking coupled walls with innovative Resilient Slip Friction (RSF) joints. Journal of Constructional Steel Research 129: 215–226.

Hashemi A, Zarnani P, Masoudnia R, Quenneville P. 2018. Experimental testing of rocking cross-laminated timber walls with resilient slip friction joints. Journal of Structural Engineering 144: 04017180.

Kashani MM, Gonzalez-Buelga A, Thayalan RP, Thomas AR, Alexander NA. 2018. Experimental investigation of a novel class of self-centring spinal rocking column. Journal of Sound and Vibration 437: 308–324.

Kiggins, S., Uang, C.-M. 2006. Reducing residual drift of buckling-restrained braced frames as a dual system. Eng. Struct., 28(11), 1525–1532.10.1016/j.engstruct.2005.10.023

Lignos, D., Elkady, A. Effect of gravity framing on the overstrength and collapse capacity of steel frame buildings with perimeter special moment frames, *Earthquake Engineering and Structural Dynamics*, Vol 44 (8), pp 1289-1307, 2015.

Ma XH, Krawinkler G, Deierlein G. 2011. Seismic design and behaviour of self-centering braced frames with controlled rocking and energy dissipating fuses. Report No. 174. Stanford, CA: Stanford University

Ma, J-L., Chan, T-M., Young, B. 2017. Tests on high-strength steel hollow sections: a review, Structures and Buildings, Vol 170 (SB9), Pages 621-630, DOI: doi/10.1680/jstbu.16.00113

MacRae, G. A., Kawashima, K. 1998. Post-earthquake residual displacements of bilinear oscillators, *Earthquake Engineering and Structural Dynamics*, 26(7), 701-716.

Mansour, N., Christopoulos, C., Tremblay, R. 2011. Experimental validation of replaceable shear links for eccentrically braced steel frames, ASCE Journal of Structural Engineering. 137(10): 1141-1152.

McCormick, J., Aburano, H., Ikenaga, M., and Nakashima, M. 2008. Permissible residual deformation levels for building structures considering both safety and human elements. *Proc. 14th World Conf. EE*, China, Beijing, Paper ID 05-06-0071.

McKenna F, Fenves GL, Scott MH. Open system for earthquake engineering simulation. [Computer Software], Pacific Earthquake Engineering Research Center, University of California, Berkeley, CA. 2000. http://opensees.berkeley.edu

Miller DJ, Fahnestock LA, Eatherton MR. 2012. Development and experimental validation of a nickel–titanium shape memory alloy self-centering buckling-restrained brace. Engineering Structures 40: 288–298.

Miranda, E., Ruiz-Garcia, J. Evaluation of approximate methods to estimate maximum inelastic displacement demands, *Earthquake Engineering and Structural Dynamics*, Vol 31, pp 539-560, 2002.

Mojiri, S., Mortazavi, P., Kwon, O., Christopoulos, C. 2021. Seismic response evaluation of a five-story buckling-restrained braced frame using multi-element pseudo-dynamic hybrid simulations, *Earthquake Engineering and Structural Dynamics*, 50(12), 3243-3265. DOI: https://doi.org/10.1002/eqe.3508.

Mortazavi, P. 2023. Large-scale experimental validation and design of resilient EBFs with cast steel replaceable modular yielding links, PhD Dissertation, Department of Civil and Mineral Engineering, University of Toronto.

Mortazavi, P., Lee, E., Binder, J., Kwon, O., Christopoulos, C. 2023s. Large-Scale Experimental Validation of Optimized Cast Steel Replaceable Modular Yielding Links for Eccentrically Braced Frames, *ASCE Journal of Structural Engineering,* **149** (7), DOI: https://doi.org/10.1061/JSENDH.STENG-1163.

Mortazavi, P., Binder, J., Kwon, O., Christopoulos, C. 2023b. Ductility-Targeted Design of Cast Steel Replaceable Modular Yielding Links and their Experimental Validation through Large-Scale Testing, *ASCE Journal of Structural Engineering,* **149** (7), DOI: https://doi.org/10.1061/JSENDH.STENG-12097.

Mortazavi, P., Kwon, O., Christopoulos, C. 2023c. Pseudo-dynamic hybrid simulations on steel eccentrically braced frames equipped with cast steel replaceable modular yielding links, *Earthquake Engineering and Structural Dynamics*, 52 (12), 3622-3648. DOI: https://doi.org/10.1002/eqe.3923.

Mortazavi, P., Kwon, O., Christopoulos, C. (2024a). Seismic Performance of Steel Eccentrically Braced Frames with Conventional and Replaceable Yielding Links Designed with ASCE 7-16, *ASCE Journal of Structural Engineering.* **150** (5), DOI: https://doi.org/10.1061/JSENDH.STENG-13093

Mortazavi, P., Christopoulos, C., Kwon, O. (2024b). Mitigation of residual deformations in eccentrically braced frames through a low-cost re-centering mechanism, *Earthquake Engineering and Structural Dynamics*, **53** (7), 2255-2282. DOI: https://doi.org/10.1002/eqe.4113

Mortazavi, P., Kwon, O., Christopoulos, C. 2022. Four-Element Pseudodynamic Hybrid Simulation of a Steel Frame with Cast Steel Yielding Connectors under Earthquake Excitations, *ASCE Journal of Structural Engineering.* **148** (2). DOI: https://doi.org/10.1061/(ASCE)ST.1943-541X.0003232.

Ocel J, DesRoches R, Leon RT, Hess WG, Krumme R, Hayes JR, Sweeney S. 2004. Steel beam-column connections using shape memory alloys. Journal of Structural Engineering 130(5):732–740.

Ozbulut OE, Hurlebaus S. 2010. Seismic assessment of bridge structures isolated by a shape memory alloy/rubber-based isolation system. Smart Materials and Structures 20(1): 015003.

Pampanin, S., Christopoulos, C., Priestley, N. 2003. Performance-based seismic response of frame structures including residual deformations. Part II: Multi-degree of freedom systems, Journal of Earthquake Engineering, Vol (7), No. 1, 119-147.

PEER Ground Motion database. Pacific Earthquake Engineering Research Center. http://ngawest2.berkeley.edu [2015]

Qian H, Li H, Song G. 2016. Experimental investigations of building structure with a superelastic shape memory alloy friction damper subject to seismic loads. Smart Materials and Structures 25(12): 125026.

Ruiz-Garcia, J., Miranda, E. Inelastic displacement ratios for evaluation of existing structures, *Earthquake Engineering and Structural Dynamics*, Vol 32, pp 1237-1258, 2003.

Sabelli, R., Mahin, S., and Chang, C. 2003. Seismic demands on steel braced frame buildings with buckling restrained braces. *Eng. Struct.*, 25(5), 655–666.10.1016/S0141-0296(02)00175-X

Tremblay, R., Lacerte, M., and Christopoulos, C. 2008. Seismic response of multistory buildings with self-centering energy dissipative steel braces. J. Struct. Eng., 134(1), 108–120.10.1061/(ASCE)0733-9445(2008)134:1(108)

Wiebe L, Christopoulos C. 2015. Performance-based seismic design of controlled rocking steel braced frames. I: Methodological framework and design of base rocking joint. Journal of Structural Engineering 141(9): 04014226.

Xu L, Xiao S, Li Z. 2018. Hysteretic behavior and parametric studies of a self-centering RC wall with disc spring devices. Soil Dynamics and Earthquake Engineering 115: 476–488.

Youssef MA, Alam MS, Nehdi M. 2008. Experimental investigation on the seismic behavior of beam-column joints reinforced with superelastic shape memory alloys. Journal of Earthquake Engineering 12(7): 1205–1222.

Zareie S, Issa AS, Seethaler RJ, Zabihollah A. 2020. Recent advances in the applications of shape memory alloys in civil infrastructures: A review. Structures 27: 1535–1550.

Zhang Y, Zhu S. 2007. A shape memory alloy-based reusable hysteretic damper for seismic hazard mitigation. Smart Materials and Structures 16(5): 1603

Zhong, M., Christopoulos, C. 2021. Self-Centering Seismic-Resistant Structures: Historical Overview and State-of-the-Art, Earthquake Spectra, Vol 38 (2), 1321-1356.